Collisional redistribution of hydrogen line radiation in low- and moderate-density magnetized plasmas

J. Rosato ◉*

Aix-Marseille Université, CNRS, PIIM UMR 7345, Campus de Saint-Jérôme, Case 232, F-13397 Marseille Cedex 20, France

A computer simulation technique has been applied to the modeling of radiation redistribution functions in low- and moderate-density magnetized hydrogen plasmas. The radiating dipole is described within the Heisenberg picture, and perturbations by the plasma microfield are accounted for through a time-dependent Stark effect term in the Hamiltonian. Numerical applications are presented for the first Lyman and Balmer lines at plasma conditions relevant to tokamak divertors and magnetized white dwarf atmospheres. In both cases, the collisional redistribution of the radiation frequency is shown to be incomplete. Comparisons with a previously developed impact model are performed, and results are discussed.

I. INTRODUCTION

In plasma physics, the process of radiation scattering is described by a redistribution function $R(\omega, \vec{n}, \omega', \vec{n}')$: This quantity is the joint probability density for an atom absorbing a photon with frequency ω' and direction $\vec{n}'$ and reemitting it with frequency ω and direction $\vec{n}$. Redistribution function models are widely used in astrophysics for the description of spectral line formation from stellar atmospheres out of local thermodynamic equilibrium [1–4]. In regimes where collisions between the radiator and the plasma particles are frequent, the reemitted photon loses memory of the state of the incoming photon and the corresponding emission line shape function is identical to the absorption line shape function [1,5]; this situation is referred to as complete redistribution. In a more general case, the reemitted radiation spectrum presents a more elaborated structure, which is closely related to the shape of the redistribution function $R(\omega, \vec{n}, \omega', \vec{n}')$. Most of the current models for redistribution functions involve the Hummer R functions (R_I, R_{II} etc.) [6] and derived expressions, which account for collisional redistribution, coherent scattering, and Doppler redistribution due to the thermal motion of the atoms. One main advantage of these functions is that they involve analytical expressions or integrals that can be evaluated numerically within a reasonable CPU time; applications include inertial fusion [7] and related research works in astrophysics (e.g., see Refs. [8–10] for reviews), laboratory plasma experiments [11,12], and general transport theory [13,14]. In each of these domains, the radiation field is investigated based on a numerical solving of the radiative transfer equation and redistribution functions occur therein through an integral scattering term. In support of these radiation transport calculations, efforts have been undertaken in order to provide more accurate models for the redistribution functions. The approaches are similar to those involved in one-photon Stark line shape modeling. They include the

impact approximation [15,16] and its extensions, either based on refined collision operators [17] or on kinetic equations [18–20], and they include stochastic approaches, such as the model microfield method [21] and the frequency fluctuation model [22,23]. Computer simulations involving a numerical solving of the time-dependent Schrödinger equation have also been performed, but the literature on the subject is rather scarce. Some articles published a few decades ago were devoted to the calculation of Lyman α in specific dense plasma conditions [24,25]; a focus was put on the investigation of interference effects, and a conclusion was that the redistribution is incomplete. In the present paper, we present a new simulation method, and we apply it to the modeling of hydrogen line redistribution functions in typical plasma conditions found in magnetic fusion experiments and in magnetized white dwarf atmospheres. In the magnetic fusion framework, the motivation for this paper is the need of accuracy in transport codes. At the edge of several tokamaks, the so-called divertor region contains a cold plasma in recombining regime (typically $T_e <$ 5 eV and $N_e > 10^{14}$ cm^{-3}), which is affected by significant radiation trapping at frequencies near the hydrogen Lyman series; these opacity effects have been demonstrated both experimentally and numerically [26–31]. In the framework of ITER preparation, simulations of the Lyman line radiation transport in the divertor have shown that the opacity provides a significant additional source of excited atoms, which can affect the plasma ionization-recombination balance. Whereas modeling efforts have been devoted to the improvement of photon absorption cross sections (e.g., see Ref. [32] for a recent report), the study of the photon scattering process and its related redistribution function has been left pending. The radiative transfer simulations reported in Refs. [29–32] were performed within the complete redistribution approximation, i.e., assuming that the frequency and the direction of a photon outgoing from a scattering process are independent of those of the incoming photon. Although convenient for calculations, the complete redistribution approximation is not systematically valid in tokamak edge plasma conditions. A preliminary investigation [33], based on the

---

*joel.rosato@univ-amu.fr

impact approximation for ions, has indicated that the Zeeman effect introduces nontrivial partial redistribution effects on Lyman α. Here, we reconsider this problem and address the collisional redistribution of the Lyman radiation in optically thick divertor conditions using numerical simulations. Motivated by recent studies in astrophysics [34], we also apply numerical simulations to the calculation of the redistribution functions involved in the formation of Balmer lines in white dwarf atmosphere conditions. The article is organized as follows: In Sec. II, a brief presentation of the radiation transport formalism is given, highlighting how the redistribution function does explicitly appear inside the radiative transfer equation. The modeling of redistribution function is next addressed in Sec. III. The formalism involves the quantum radiation theory. Various equations are introduced and discussed. In Sec. IV, numerical calculations of the first Lyman lines are performed in optically thick divertor plasma conditions. The analytical model previously developed in Ref. [33] is next reexamined and compared to numerical simulations in Sec. V. Technical details relative to this model are given in the Appendix. In Sec. VI, the redistribution function of Balmer lines is calculated in magnetic white dwarf atmosphere conditions. Finally, a conclusion is given in Sec. VII.

II. RADIATIVE TRANSFER FORMALISM

The formalism involved in radiative transfer investigations can be found in textbooks, e.g., Refs. [1,5]. Here, a brief presentation is given. Consider a set of atoms immersed in a plasma, emitting and absorbing radiation in spectral lines. The radiative transfer equation reads

$$\left(\frac{\partial}{\partial t} + \vec{n} \cdot \vec{\nabla} \right) I = \eta - \kappa I, \tag{1}$$

where $I \equiv I(\omega, \vec{n}, \vec{r}, t)$ is the radiation specific intensity at location $\vec{r}$, at time t, at frequency ω, and in direction $\vec{n}$, and $\eta \equiv \eta(\omega, \vec{n}, \vec{r}, t)$, $\kappa \equiv \kappa(\omega, \vec{n}, \vec{r}, t)$ are the emission and absorption coefficients, respectively. The polarization states can be retained through the use of the Stokes parameters together with a suitable modification of Eq. (1); we will not consider this issue in the following, since our concern will be the modeling of the emission coefficient rather than the solving of the transport equation by itself. For the sake of simplicity, the $\vec{r}$ and t dependences are not written explicitly hereafter. The emission and absorption coefficients are given by

$$\eta = \sum_{u>l} \frac{\hbar \omega_{ul} A_{ul}}{4\pi} N_u \phi_{ul}, \tag{2}$$

$$\kappa = \sum_{u>l} \frac{\hbar \omega_{ul}}{4\pi} (N_l B_{lu} - N_u B_{ul}) \phi_{ul}. \tag{3}$$

In these expressions, the sums are carried out over the upper and lower levels u, l that contribute to the line radiation; ω_{ul} is the corresponding Bohr frequency; A_{ul}, B_{ul}, and B_{lu} are the related Einstein coefficients; $\phi_{ul} \equiv \phi_{ul}(\omega, \vec{n})$ is the line shape function, which denotes the probability density of emitting or absorbing a photon with frequency ω in the direction $\vec{n}$ [normalization convention: $\int d\omega \int d\Omega \, \phi_{ul}(\omega, \vec{n}) = 4\pi$]; and N_u, N_l are the density of atoms in the upper and lower levels. The negative contribution in Eq. (3) denotes stimulated

emission. In the expressions (2) and (3), it is implied that the redistribution is complete, i.e., the frequencies and directions of emitted and absorbed photons are assumed independent of each other. In order to account for partial redistribution, one has to perform the following substitution:

$$N_u \phi_{ul} \to N_u^* \phi_{ul}$$
$$+ \frac{N_l B_{lu}}{\Gamma_u} \int d\omega' \int d\Omega' R_{ul}(\omega, \vec{n}, \omega', \vec{n}') I(\omega', \vec{n}')$$
$$\equiv N_u \psi_{ul}, \tag{4}$$

at each place where the product $N_u \phi_{ul}$ occurs. The quantity N_u^* denotes the density of atoms excited by collisions; Γ_u is the total depopulation rate of level u, which includes both collisions and radiation; and $R_{ul}(\omega, \vec{n}, \omega', \vec{n}')$ is the redistribution function, which denotes the joint probability density of absorbing a photon with frequency ω' in the direction $\vec{n}'$ and reemitting it with frequency ω in the direction $\vec{n}$, with the normalization convention $\int d\omega \int d\Omega \int d\omega' \int d\Omega' R_{ul}(\omega, \vec{n}, \omega', \vec{n}') = (4\pi)^2$. The function ψ_{ul} present on the right-hand side is usually referred to as emission profile to be distinguished from the absorption profile ϕ_{ul}. These two profiles are identical if redistribution is complete. Also, the redistribution function factorizes as $R_{ul}(\omega, \vec{n}, \omega', \vec{n}') \equiv \phi_{ul}(\omega, \vec{n}) \phi_{ul}(\omega', \vec{n}')$ if redistribution is complete. In the following, we address the modeling of the redistribution function in a more general case where the redistribution can be partial.

III. REDISTRIBUTION FUNCTION MODELING

The two main causes for radiation redistribution are the collisions with perturbers and the Doppler effect relative to the thermal motion of the atom. The latter is usually described through a convolution with the atomic velocity distribution function [6]. Since it involves no major difficulties (apart from the numerical computation by itself), we do not consider this effect and focus on the modeling of the redistribution function in the atomic frame of reference, i.e., without Doppler broadening. Correlations between the Doppler effect and the collisions will not be addressed as well since they are not essential to the investigation presented hereafter (if required, they can be retained using the same method as that for one-photon line shape modeling [35]). Various approaches to the modeling of collisional redistribution have been reported in the literature, e.g., Refs. [2,15–25]. For convenience, and by consistency with already available line shape codes, we here use the same terminology as in Stark broadening modeling, along the lines of review articles and textbooks [36–39]. The emission line shape ψ_{ul} in Eq. (4) is proportional to the power spectrum $P(\omega)$ radiated from a single atom. According to quantum electrodynamics, this quantity is given by the following relation:

$$P(\omega) = \frac{\omega^4}{3\pi \varepsilon_0 c^3} F(\omega), \tag{5}$$

$$F(\omega) = \lim_{T \to \infty} \frac{1}{2\pi T} \langle \tilde{\vec{d}}^{(-)}(-\omega, T) \cdot \tilde{\vec{d}}^{(+)}(\omega, T) \rangle, \tag{6}$$

with

$$\tilde{\vec{d}}^{(\pm)}(\pm\omega, T) = \int_0^T dt \, e^{\pm i\omega t} \vec{d}^{(\pm)}(t). \tag{7}$$

The quantities $\vec{d}^{(+)}(t)$ and $\vec{d}^{(-)}(t)$ denote the positive and negative frequency contributions to the dipole operator expressed in the Heisenberg picture, and the brackets denote an average carried out over the atomic states, the perturbers, and the radiation field. Equation (6) holds for line radiation, i.e., it is assumed that the characteristic frequency ω of the radiated field is much larger than the characteristic spectral band. As in Ref. [36], we refer to the quantity $F(\omega)$ as the line shape function. An explicit evaluation of this quantity requires a model for the time evolution of the dipole operator. If the redistribution is complete, the following Heisenberg equation of motion can be used ($\hbar \equiv 1$ is set):

$$\dot{\vec{d}}^{(+)} = i[H_A + V, \vec{d}^{(+)}], \qquad (8)$$

and the usual one-photon line shape formalism applies; here, H_A is the atomic Hamiltonian and $V = -\vec{d} \cdot \vec{E}_{\mathrm{plasma}}$ is the Stark perturbation due to the plasma microfield $\vec{E}_{\mathrm{plasma}}$. By convention, a Zeeman effect term is included in H_A if a magnetic field is present. If the redistribution is partial, Eq. (8) must be modified in such a way so as to account for the quantized (transverse) electric field $\vec{E}_R$. The latter involves one contribution $\vec{E}_{\mathrm{in}}$, corresponding to the incoming photon and another one $\vec{E}_{\mathrm{out}}$, corresponding to the reemitted photon; namely, one has $\vec{E}_R \equiv \vec{E}_{\mathrm{in}} + \vec{E}_{\mathrm{out}}$. In a classical electromagnetism framework, these contributions correspond to the solution of the Maxwell equation set in the absence of source and the solution in the presence of an oscillating dipole, respectively. Both must be retained for a consistent description of the scattering process. The term $\vec{E}_{\mathrm{out}}$ contributes to the radiative width and (Lamb) shift. A proper accounting for these two effects within the Heisenberg picture has already been discussed, e.g., see Refs. [40–45]. A practical implementation consists, first, in defining a new effective atomic Hamiltonian $\bar{H}_A$, which includes a non-Hermitian term,

$$\bar{H}_A = H_A - iK_{\mathrm{rad}}. \qquad (9)$$

The operator K_{rad} is assumed diagonal in the atomic Hamiltonian base; it is given by

$$\langle j|K_{\mathrm{rad}}|j\rangle = \sum_{k<j} \frac{\omega_{jk}^3 |\langle j|\vec{d}(0)|k\rangle|^2}{6\pi\varepsilon_0 c^3} \equiv \sum_{k<j} \frac{A_{jk}}{2}, \qquad (10)$$

where A_{jk} is the Einstein coefficient corresponding to the $j \rightarrow k$ radiative transition. The next step consists in replacing the commutator $[H_A, \vec{d}^{(+)}]$ present in Eq. (8) by the following expression:

$$\bar{H}_A^\dagger \vec{d}^{(+)} - \vec{d}^{(+)} \bar{H}_A. \qquad (11)$$

Introducing the interaction term $-\vec{d} \cdot \vec{E}_{\mathrm{in}}$ and applying the rotating wave approximation, which holds for near-resonant radiation [43–45], one obtains the following equation of motion for the dipole:

$$\dot{d}_a^{(+)} = i(\bar{H}^\dagger d_a^{(+)} - d_a^{(+)}\bar{H}) + i\sum_b [d_a^{(+)}, d_b^{(-)}]E_{\mathrm{in},b}^{(+)}, \qquad (12)$$

where the a and b indices denote x, y, and z components, $\bar{H} = \bar{H}_A + V$, and $E_{\mathrm{in},b}^{(+)}$ refers to the positive frequency component of the field $\vec{E}_{\mathrm{in}}$. Equation (12) will be used in substitution of

Eq. (8) for the modeling of the dipole evolution with partial radiation redistribution. In order to get a solution, we assume the field act as a weak perturbation on the atomic system and apply a linearization procedure. The dipole operator at first order reads

$$d_{1,a}^{(+)}(t) = i\int_0^t dt' \bar{U}_l^\dagger(t', t)$$
$$\times \sum_b [d_{0,a}^{(+)}(t'), d_{0,b}^{(-)}(t')]E_b^{(+)}(t')\bar{U}_u(t', t). \qquad (13)$$

The shortcut notation $E_{\mathrm{in},b}^{(+)} \equiv E_b^{(+)}$ has been used here. The quantities $\bar{U}_l(t', t)$ and $\bar{U}_u(t', t)$ denote propagators acting on states in the lower and upper levels relative to the transition under consideration, respectively. They obey the time-dependent Schrödinger equation,

$$\frac{\partial}{\partial t}\bar{U}_{u,l}(t', t) = -i\bar{U}_{u,l}(t', t)\bar{H}_{u,l}(t), \qquad (14)$$

with the initial condition $\bar{U}_{u,l}(t', t') = 1$ and with the condition $t' \leqslant t$. The Hamiltonians $\bar{H}_{u,l}$ are the projections of $\bar{H}$ onto the upper and lower levels and taken at initial time, i.e., expressed in the Schrödinger picture. The identity $\bar{H}^\dagger d_a^{(+)} - d_a^{(+)}\bar{H} \equiv \bar{H}_l^\dagger d_a^{(+)} - d_a^{(+)}\bar{H}_u$ has been used here; it holds within the no-quenching approximation where inelastic collisions are neglected. This approximation (commonly used in line broadening modeling [39]) is suitable here, in particular, due to the energy level degeneracy of the hydrogen atom. In Eq. (13), the quantities $d_{0,a}^{(+)}(t')$ and $d_{0,b}^{(-)}(t')$ correspond to the zeroth-order "bare" solutions of the equation of motion, i.e., in the absence of radiation damping. They are given by

$$d_{0,a}^{(+)}(t') = U_l^\dagger(0, t')d_a^{(+)}(0)U_u(0, t'), \qquad (15)$$

$$d_{0,b}^{(-)}(t') = U_u^\dagger(0, t')d_b^{(-)}(0)U_l(0, t'), \qquad (16)$$

where the corresponding propagators obey the time-dependent Schrödinger equation associated with the bare Hamiltonian $H = H_A + V$,

$$\frac{\partial}{\partial t}U_{u,l}(t', t) = -iU_{u,l}(t', t)H_{u,l}(t). \qquad (17)$$

Because of the no-quenching approximation, the propagators $\bar{U}_{u,l}(t', t)$ only act on the operator $d_{0,a}^{(+)}$ that occurs in Eq. (13). Ignoring entanglement between Stark broadening and radiation damping due to time ordering, we use the following approximation:

$$\bar{U}(t', t) \simeq U(t', t)e^{-K_{\mathrm{rad}}(t-t')}. \qquad (18)$$

This approximation holds in regimes where the radiative damping is weak compared to the other line broadening mechanisms. A similar factorization procedure is sometimes used in Stark broadening simulations (albeit in another context: the factorization concerns the ionic and electronic contributions to the evolution operator, e.g., see Ref. [46] for details).

From Eq. (18), one can rewrite the first-order dipole as

$$d_{1,a}^{(+)}(t) = i \int_0^t dt' \sum_b [e^{-K_{\mathrm{rad},l}(t-t')} d_{0,a}^{(+)}(t) e^{-K_{\mathrm{rad},u}(t-t')}, d_{0,b}^{(-)}(t')] E_b^{(+)}(t'). \tag{19}$$

The radiated power spectrum is obtained by using this expression for the dipole in the formulas (5)–(7). Since the positive and negative frequency components $\vec{d}_0^{(+)}$ and $\vec{d}_0^{(-)}$ act on the lower-energy atomic states on the left (bra) and right (ket) sides, respectively, the following substitution can be performed in Eq. (19):

$$[e^{-K_{\mathrm{rad},l}(t-t')} d_{0,a}^{(+)}(t) e^{-K_{\mathrm{rad},u}(t-t')}, d_{0,b}^{(-)}(t')]$$
$$\rightarrow e^{-K_{\mathrm{rad},l}(t-t')} d_{0,a}^{(+)}(t) e^{-K_{\mathrm{rad},u}(t-t')} d_{0,b}^{(-)}(t'), \tag{20}$$

and the final result becomes simpler. For completeness, we now write the radiation field operator explicitly,

$$\vec{E}^{(+)}(t') = -i \sum_{\vec{k}'', \vec{\varepsilon}''} \sqrt{\frac{\omega''}{2\varepsilon_0 V}} a_{\vec{k}'', \vec{\varepsilon}''}(0) e^{-i\omega'' t'} \vec{\varepsilon}''. \tag{21}$$

The sum is carried out over the modes $(\vec{k}'', \vec{\varepsilon}'')$, $\omega'' = |\vec{k}''|c$ is the corresponding frequency, $a_{\vec{k}'', \vec{\varepsilon}''}(0)$ is the annihilation operator at initial time, and V is the quantization volume. The occurrence of $a_{\vec{k}'', \vec{\varepsilon}''}(0)$ can be eliminated formally through expressing the statistical average in Eq. (6) explicitly in terms of the density operator ρ. Assuming weak coupling, we write it in factorized form as

$$\rho = \rho_A \otimes \rho_P \otimes |1_{\vec{k}', \vec{\varepsilon}'}\rangle \langle 1_{\vec{k}', \vec{\varepsilon}'}|, \tag{22}$$

where $\rho_A = \sum_\beta |\beta\rangle\langle\beta|$ involves the initial (lower-energy) atomic states contributing to the scattering, ρ_P involves the plasma variables, and $|1_{\vec{k}', \vec{\varepsilon}'}\rangle \langle 1_{\vec{k}', \vec{\varepsilon}'}|$ refers to the one-photon state relative to the incoming radiation. The implementation of the expression (22) inside the statistical average (6) makes the following identities $\langle 1_{\vec{k}', \vec{\varepsilon}'}| a_{\vec{k}'', \vec{\varepsilon}''}^\dagger(0) = \delta_{\vec{k}', \vec{k}''} \delta_{\vec{\varepsilon}', \vec{\varepsilon}''} \langle 0|$ and $a_{\vec{k}'', \vec{\varepsilon}''}(0)|1_{\vec{k}', \vec{\varepsilon}'}\rangle = \delta_{\vec{k}', \vec{k}''} \delta_{\vec{\varepsilon}', \vec{\varepsilon}''}|0\rangle$ appear, which eliminates the field operators. Now, define the following two quantities:

$$\vec{D}^{(+)}(t)$$
$$= \int_0^t dt' e^{-K_{\mathrm{rad},l}(t-t')} \vec{d}_0^{(+)}(t) e^{-K_{\mathrm{rad},u}(t-t')} \vec{d}_0^{(-)}(t') \cdot \vec{\varepsilon}' e^{-i\omega' t'},$$
$$\tag{23}$$

$$\vec{D}^{(-)}(t) = [\vec{D}^{(+)}(t)]^\dagger, \tag{24}$$

the line shape function reads

$$F(\omega) = \frac{\omega'}{2\varepsilon_0 V} \lim_{T \to \infty} \frac{1}{2\pi T} \langle \tilde{\vec{D}}^{(-)}(-\omega, T) \cdot \tilde{\vec{D}}^{(+)}(\omega, T) \rangle, \tag{25}$$

where $\tilde{\vec{D}}$ is a Fourier transform of $\vec{D}$ from Eq. (23), similar to Eq. (7). This formula will serve as a basis in the calculations presented hereafter. The redistribution function introduced in Eq. (4) can be obtained from $F(\omega)$ through normalization and summation over the polarization states [note that the quantities $\vec{D}^{(\pm)}(t)$, $\tilde{\vec{D}}^{(\pm)}(\pm\omega, T)$, and $F(\omega)$ depend on the incoming photon frequency ω' through the exponential term $e^{-i\omega' t'}$ present in Eq. (23)]. Since the average over the one-photon state $|1_{\vec{k}', \vec{\varepsilon}'}\rangle$ has been performed explicitly, the brackets now denote a statistical average over the atomic states and the plasma variables only.

IV. APPLICATION TO LYMAN LINES IN OPTICALLY THICK DIVERTOR PLASMAS

The line shape function $F(\omega)$ given in Eq. (25) has been calculated numerically for Lyman lines in conditions typical of optically thick divertor plasmas. The numerical method involves an integration of the Schrödinger Eq. (17), an evaluation of the matrix products (15) and (16), and an evaluation of the integral (23). The Fourier transform (7) has also been performed numerically; the upper bound T has been chosen sufficiently large so as to obtain convergence in the result. The microfield $\vec{E}_{\mathrm{plasma}}$ has been evaluated from a simulation of the perturber trajectories. In this simulation, the plasma particles are left moving near the atom in a cubic box with periodic boundary conditions. This method is precisely the same as that used in Stark-broadened one-photon line shape calculations, e.g., see Refs. [47–54] for details. The Schrödinger Eq. (17) is also identical to that employed in one-photon line shape calculations and can be addressed with the same algorithms. Both ions and electrons have been retained here. In order to reduce the noise, several runs corresponding to different initial conditions have been performed. Figure 1 shows a plot of the line shape function $F(\omega)$ for Lyman α, assuming pure hydrogen plasma with $N_e = 10^{14}$ cm^{-3} and $T_e = T_i = 1$ eV. The incoming photon frequency detuning $\Delta\omega' = \omega' - \omega_{\mathrm{Ly}\alpha}$ has been set equal to 5×10^{-5} eV. This value is on the order of the line width, hence, it is representative of the characteristic energy of an incoming Lyman α photon produced by
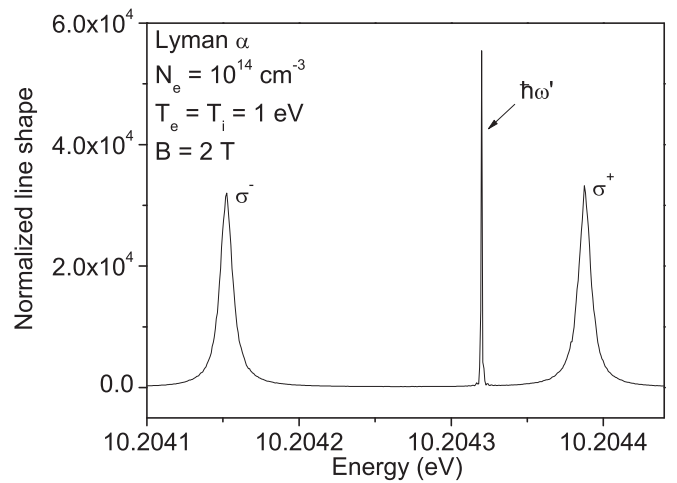

FIG. 1. Plot of the Lyman α line shape function $F(\omega)$ normalized to unity. A numerical simulation method has been used. Both resonance fluorescence and Rayleigh components are visible in the spectrum, which indicates that the radiation redistribution is incomplete. Only the σ components of the spectrum are shown here for the sake of clarity.
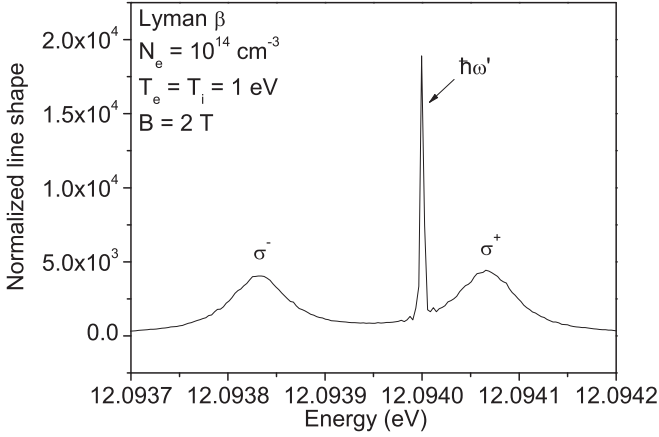
FIG. 2. Plot of the Lyman β line shape function for the same conditions as in Fig. 1. The redistribution is also incomplete. The Zeeman components are broader than those of Lyman α because the Stark effect is more important for this line.

emission from another atom. An external magnetic field of 2 T has been assumed. A linear polarization, perpendicular to $\vec{B}$, has been assumed for the incoming photon. In order to clarify the figure, only the σ components of the spectrum, i.e., those involving the selection rule $\Delta m_l = \pm 1$, are shown. As can be seen in the figure, the spectrum presents three components. The two lateral components coincide with the normal Zeeman spectrum observed parallel to $\vec{B}$. They denote resonance fluorescence: the atomic upper levels have been populated through excitation by the incoming radiation field together with elastic collisions with the plasma particles. The third component is located at the position of the incoming photon frequency. It is interpreted as coherent Rayleigh scattering and it indicates that part of the radiation has not been redistributed by collisions. The redistribution is also partial for Lyman β. Figure 2 shows the result of a calculation performed in the same conditions. The fluorescence components are broader in this case because the Stark effect is more important for this line.

V. ANALYSIS OF A PREVIOUSLY DEVELOPED IMPACT MODEL

An analytical model for the Lyman α redistribution function, suitable for fast evaluation in a radiation transport code, was developed in Ref. [33]. The model involves the impact approximation for ions; in this framework, the line shape is given by the following formula:

$$F(\omega) = \frac{\pi \omega'}{2\varepsilon_0 V} \sum_{\alpha,\beta} \frac{p_\beta C_{\alpha\beta}}{\Gamma_{\alpha\beta} \Gamma_\alpha^{\mathrm{rad}}} L(\omega' - \omega_{\alpha\beta}, \Gamma_{\alpha\beta})$$

$$\times \left[\Gamma_\alpha^{\mathrm{rad}} \delta(\omega' - \omega) + \Gamma_\alpha^{\mathrm{coll}} L(\omega - \omega_{\alpha\beta}, \Gamma_{\alpha\beta}) \right]. \quad (26)$$

The main steps in the derivation of this expression are presented in the Appendix. The sum is performed over the upper (α) and lower (β) states involved in the line, and, by definition, $C_{\alpha\beta} = |\langle \alpha | \vec{d}(0) | \beta \rangle|^2 |\langle \alpha | \vec{d}(0) \cdot \vec{\varepsilon}' | \beta \rangle|^2$, $\Gamma_\alpha^{\mathrm{rad}} = \langle \alpha | K_{\mathrm{rad}} | \alpha \rangle$, $\Gamma_{\alpha\beta}^{\mathrm{coll}} = \langle \alpha | K_{\mathrm{coll}} | \alpha \rangle + \langle \beta | K_{\mathrm{coll}} | \beta \rangle$ where K_{coll} is the collision operator and $L(x, \gamma) = (\gamma/\pi)/(x^2 + \gamma^2)$ is the normalized Lorentzian function. Figure 3 shows a nu-
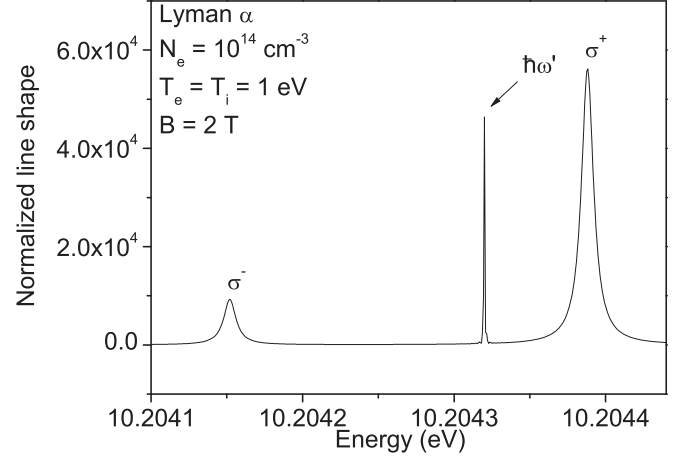

FIG. 3. Plot of the Lyman α line shape obtained from the impact model. The Zeeman components have different amplitudes, which is in contrast to the simulation result in Fig. 1. A reason for this is that interferences between the scattering amplitudes are not retained within this model. See the text for explanation.

merical application to Lyman α at the same density and temperature conditions as in the previous section. In the numerical calculation, the δ function in Eq. (26) has been replaced by the quantity $[2/\pi (\omega' - \omega)^2 t_m] \sin^2[(\omega' - \omega) t_m / 2] \equiv \delta_{1/t_m}(\omega' - \omega)$, which is expected to provide meaningful results if t_m is chosen large enough (it exactly coincides with the δ function at the $t_m \to \infty$ limit). Here, this time has been set equal to the simulation time used in Fig. 1; its value is $t_m = 4.4 \times 10^{-9}$ s. The collision operator K_{coll} has been evaluated using a variant of the Griem-Baranger-Kolb-Oertel model [55], designed to account for the Zeeman degeneracy removal. As can be seen in the figure, the redistribution is incomplete as in the simulation result in Fig. 1, but the relative amplitude of the Zeeman components is different. The σ^+ component appears much higher than the σ^- component. An interpretation for this is that the atom has more probability
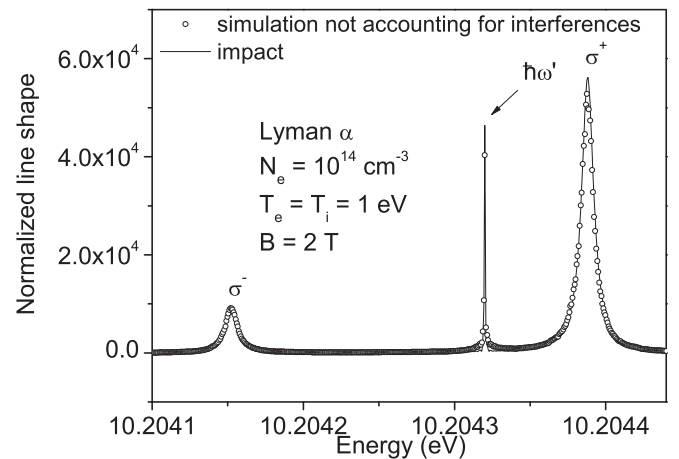

FIG. 4. If the interferences between the scattering amplitudes are removed from the simulation, the two results are in agreement with each other. Here, the Lyman α line shape has been calculated with the same conditions as in Figs. 1 and 3.
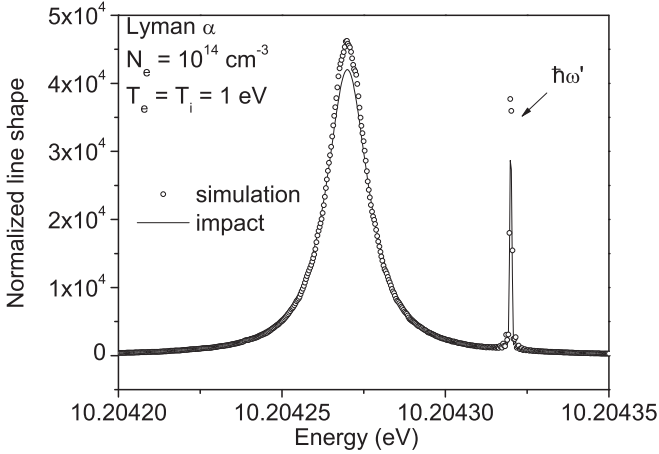
FIG. 5. The Stark widths obtained from the impact model and the simulation are also in good agreement. Here, the simulation and impact results are plotted for the same plasma conditions. For the sake of clarity, the magnetic field has been set equal to zero.

to be pumped in the $m_l = 1$ Zeeman sublevel than in the $m_l = -1$ sublevel if the impact model is used. This deviation stems from the neglect of interferences between the scattering amplitudes in Eq. (26). Transitions, such as $|1s\rangle \rightarrow |2p_1\rangle \rightarrow |1s\rangle$, $|1s\rangle \rightarrow |2p_{-1}\rangle \rightarrow |1s\rangle$ are susceptible to interfere with each other, resulting in an increase in the probability for the atom to reemit radiation from a sublevel far from the excitation. In contrast, by construction, the simulation accounts for such interferences. Figure 4 illustrates this point. We have artificially removed these interferences from the simulation by dropping the off-diagonal matrix elements of the evolution operator at the stage of evaluating the integral (23). The results are now in agreement with each other. It is worth noting that the Stark widths obtained from the impact model and the simulation are also in good agreement. This is magnified in Fig. 5. The simulation and impact results are plotted for the same plasma conditions. For the sake of clarity, the magnetic field has been set equal to zero.

VI. BALMER LINES IN MAGNETIC WHITE DWARF ATMOSPHERES

We have applied the simulation to the redistribution of Balmer lines in white dwarf atmosphere conditions. Calculations have been performed for pure hydrogen plasma at $N_e = 10^{17}$ cm^{-3} and $T_e = T_i = 1$ eV. Figure 6 shows a plot of the $H\alpha$ and $H\beta$ line shapes. The detuning $\Delta\omega'$ has been set equal to 5×10^{-3} eV for $H\alpha$ and 3×10^{-2} eV for $H\beta$. In each case, the spectrum presents the Rayleigh peak at the position of the incoming photon frequency ω', which indicates that redistribution is again incomplete. The influence of an external magnetic field is presently under investigation. In contrast to magnetic fusion experiments, the white dwarfs can have an extremely intense magnetic field (up to several kiloteslas), resulting in the occurrence of quadratic Zeeman effect and corresponding asymmetric spectra. The quadratic Zeeman effect has already been investigated in the literature [56], but elaborate line shape models accounting for this effect simultaneously with the Stark broadening are not
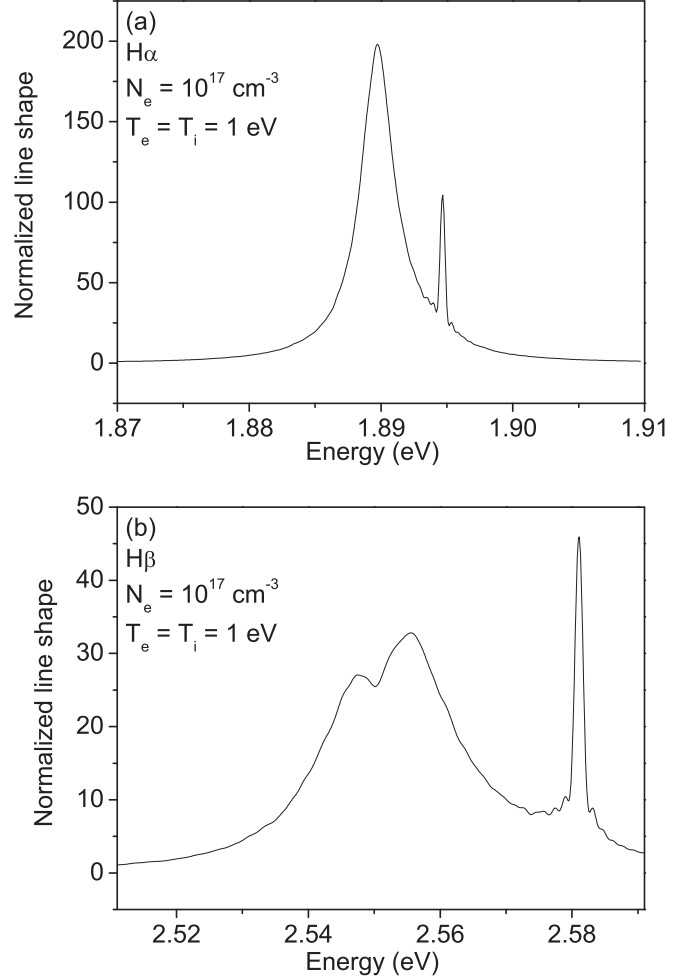

FIG. 6. Plot of the $H\alpha$ and $H\beta$ line shapes in white dwarf atmosphere conditions. The redistribution is incomplete in both cases.
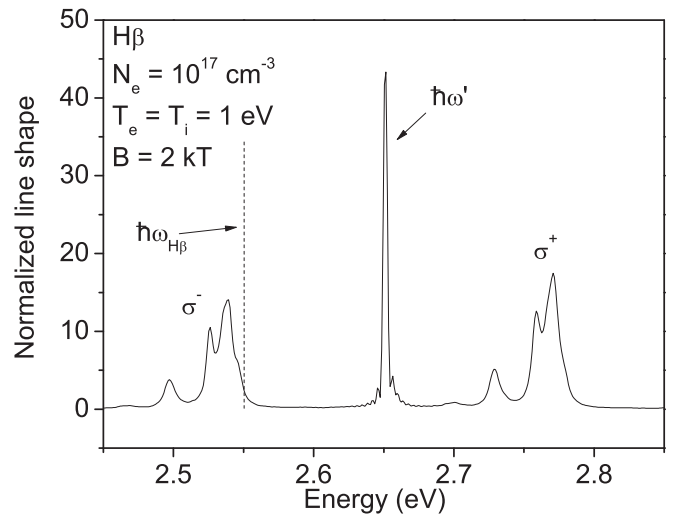

FIG. 7. White dwarfs can have a very strong magnetic spectrum, resulting in asymmetric Zeeman spectra. Here, this effect is illustrated in the case of $H\beta$ under a magnetic field of 2 kT. The quadratic Zeeman effect yields a shift of the overall line and splitting of the components. The unperturbed $H\beta$ frequency is shown as reference. The Rayleigh peak is still visible, indicating that redistribution is incomplete.

yet available; this lack concerns both one-photon line shapes and redistribution functions. An example of redistribution function with quadratic Zeeman effect is shown in Fig. 7. The $H\beta$ line shape has been calculated assuming a magnetic field value of 2 kT and taking the same values as above for the other plasma parameters. The frequency interval is larger and involves frequencies close to $H\gamma$; hence, for consistency, mixing with the $n = 5$ level has been retained in the calculation. The incoming photon frequency detuning has been set equal to 0.1 eV. As can be seen in the figure, the line shape has a complex structure. The quadratic Zeeman effect yields an overall shift of the spectrum (see the vertical dashed line for the unperturbed $H\beta$ frequency) and it provides a splitting of the components. The Rayleigh peak is still visible, indicating that redistribution is incomplete.

VII. CONCLUSION

The collisional redistribution of line radiation has been investigated in low- and moderate-density magnetized plasmas. The formalism involves an equation of motion for the atomic dipole expressed in the Heisenberg picture. In this framework, using a linearization procedure, we have derived an expression for the dipole response to the incoming photon involved in the scattering process. This response enters as an input in the radiation power spectrum formula used in line shape calculations. Using a computer simulation method, we have first applied this formula to the modeling of the collisional redistribution of the first Lyman lines in divertor plasma conditions. The obtained spectra present an unshifted component at the frequency of the incoming photon. This component is interpreted as the result of Rayleigh scattering,

and its occurrence indicates that a part of the radiation has not been redistributed by collisions. The remaining part of the spectra corresponds to resonance fluorescence induced by the collisions. A previously developed impact model has also been applied to the collisional redistribution of Lyman α. The obtained spectra are qualitatively in agreement with the simulation results, but deviations between the intensities of the Zeeman components are present. A reason for these deviations is that interferences occurring between the scattering amplitudes are not retained within the impact model. This point has been illustrated through comparison to a specific simulation where these interferences have been removed artificially. In an astrophysical framework, the collisional redistribution of radiation has next been examined through calculations of Balmer lines in white dwarf atmosphere conditions. The obtained spectra present a Rayleigh peak, indicating that the redistribution is again incomplete in such conditions. The influence of a strong magnetic field has also been illustrated through a calculation of $H\beta$ accounting for quadratic Zeeman effect. The resulting spectrum presents a complex structure, with an overall shift and an asymmetric splitting of the components. New calculations are presently underway. In the magnetic fusion framework, a refinement of the impact formula still remains to be performed. This extension should involve an implementation of the interference effects. Deviations to the impact approximation for ions, which are expected at the highest density regimes, should also be addressed, e.g., using an improved collision operator model as in Ref. [17]. In the field of dense plasma diagnostics, specific experiments with laser-plasma interactions (as recently reported in Ref. [57]) also provide motivation for the development of new redistribution function models.

APPENDIX

The analytical expression (26) has been obtained within the impact approximation. In this model, the microfield evolution timescale is assumed much shorter than the characteristic time of interest of the line. In this framework, the action of perturbers is treated as a series of binary and brief collisions. The first step in the derivation of Eq. (26) consists in rewriting the average present in Eq. (25) in terms of a four-times autocorrelation function,

$$F(\omega) = \lim_{T \to \infty} \frac{\omega'}{4\pi\varepsilon_0 V T} \int_0^T dt_4 \int_0^{t_4} dt_3 \int_0^T dt_2 \int_0^{t_2} dt_1 \, e^{i[\omega(t_2 - t_4) + \omega'(t_3 - t_1)]} C(t_2, t_1, t_4, t_3), \tag{A1}$$

$$C(t_2, t_1, t_4, t_3) \equiv \sum_{a,b,c} \varepsilon_a' \varepsilon_c' \langle e^{-K_{\mathrm{rad},l}(t_4 - t_3)} d_{0,a}^{(+)}(t_3) e^{-K_{\mathrm{rad},u}(t_4 - t_3)} d_{0,b}^{(-)}(t_4) e^{-K_{\mathrm{rad},l}(t_2 - t_1)} d_{0,b}^{(+)}(t_2) e^{-K_{\mathrm{rad},u}(t_2 - t_1)} d_{0,c}^{(-)}(t_1) \rangle. \tag{A2}$$

Similar developments were reported in the literature, e.g., Refs. [15,16]. The autocorrelation function satisfies the relation $C^*(t_2, t_1, t_4, t_3) = C(t_4, t_3, t_2, t_1)$. With this property, the contribution to Eq. (A1) from the integration domain with $t_2 > t_4$ is the complex conjugate of the contribution from $t_2 < t_4$. This justifies the replacement [16]

$$\int_0^T dt_4 \int_0^{t_4} dt_3 \int_0^T dt_2 \int_0^{t_2} dt_1 \cdots = 2 \operatorname{Re} \int_0^T dt_4 \int_0^{t_4} dt_3 \int_0^{t_4} dt_2 \int_0^{t_2} dt_1 \cdots. \tag{A3}$$

The autocorrelation function (A2) is split into three terms, which correspond to the three possible time sequences in Eq. (A1): (i) $t_1 \leqslant t_2 \leqslant t_3 \leqslant t_4$; (ii) $t_1 \leqslant t_3 \leqslant t_2 \leqslant t_4$; (iii) $t_3 \leqslant t_1 \leqslant t_2 \leqslant t_4$. The term (i) reads

$$C_{(i)} = \sum_{a,b,c} \varepsilon_a' \varepsilon_c' \langle e^{-K_{\mathrm{rad},l}\tau_3} d_{0,a}^{(+)}(t_1 + \tau_1 + \tau_2) e^{-K_{\mathrm{rad},u}\tau_3} d_{0,b}^{(-)}(t_1 + \tau_1 + \tau_2 + \tau_3) e^{-K_{\mathrm{rad},l}\tau_1} d_{0,b}^{(+)}(t_1 + \tau_1) e^{-K_{\mathrm{rad},u}\tau_1} d_{0,c}^{(-)}(t_1) \rangle, \tag{A4}$$

and, because of stationarity, it simplifies into

$$C_{(i)} = \sum_{a,b,c} \varepsilon_a' \varepsilon_c' \langle e^{-K_{\mathrm{rad},l}\tau_3} d_{0,a}^{(+)}(\tau_1 + \tau_2) e^{-K_{\mathrm{rad},u}\tau_3} d_{0,b}^{(-)}(\tau_1 + \tau_2 + \tau_3) e^{-K_{\mathrm{rad},l}\tau_1} d_{0,b}^{(+)}(\tau_1) e^{-K_{\mathrm{rad},u}\tau_1} d_{0,c}^{(-)}(0) \rangle. \tag{A5}$$

Here, by definition, $\tau_1 = t_2 - t_1$, $\tau_2 = t_3 - t_2$, and $\tau_3 = t_4 - t_3$. A further simplification consists in neglecting the nondiagonal matrix elements of the evolution operators U_u and U_l involved in Eq. (A5). The substitution $d_{0,a}^{(+)}(\tau_1 + \tau_2)e^{-K_{\text{rad},u}\tau_3}d_{0,b}^{(-)}(\tau_1 + \tau_2 + \tau_3) \rightarrow d_{0,a}^{(+)}(0)e^{-K_{\text{rad},u}\tau_3}d_{0,b}^{(-)}(\tau_3)$ can be performed in Eq. (A5). The dipole $d_{0,b}^{(-)}(\tau_3)$ and the dipole $d_{0,b}^{(+)}(\tau_1)$ do not overlap in time, hence, they can be averaged separately. We introduce collision operators $K_{\text{coll},u}$, $K_{\text{coll},l}$ relative to the upper and lower levels and assume they are diagonal. The autocorrelation function (i) reads

$$C_{(i)} = \sum_{\alpha,\beta} p_\beta C_{\alpha\beta} e^{(i\omega_{\alpha\beta} - \Gamma_{\alpha\beta})\tau_3} e^{(-i\omega_{\alpha\beta} - \Gamma_{\alpha\beta})\tau_1}, \tag{A6}$$

with

$$C_{\alpha\beta} = |\langle\alpha|\vec{d}(0)|\beta\rangle|^2 |\langle\alpha|\vec{d}(0)\cdot\vec{\varepsilon}'|\beta\rangle|^2, \tag{A7}$$

$$\Gamma_{\alpha\beta} = \langle\alpha|K_{\text{coll}} + K_{\text{rad}}|\alpha\rangle + \langle\beta|K_{\text{coll}} + K_{\text{rad}}|\beta\rangle. \tag{A8}$$

Interference terms, such as $\langle\alpha|\vec{d}(0)|\beta\rangle \cdot \langle\beta|\vec{d}(0)|\alpha'\rangle$ for $\alpha' \neq \alpha$ have been neglected. A similar treatment can be performed on the terms (ii) and (iii). The resulting autocorrelation functions read

$$C_{(ii)} = \sum_{\alpha,\beta} p_\beta C_{\alpha\beta} e^{(i\omega_{\alpha\beta} - \Gamma_{\alpha\beta})\tau_3} e^{-2\Gamma_\alpha^{\text{rad}}\tau_2} e^{(-i\omega_{\alpha\beta} - \Gamma_{\alpha\beta})\tau_1}, \tag{A9}$$

$$C_{(iii)} = \sum_{\alpha,\beta} p_\beta C_{\alpha\beta} e^{(i\omega_{\alpha\beta} - \Gamma_{\alpha\beta})\tau_3} e^{-2\Gamma_\alpha^{\text{rad}}\tau_2} e^{(i\omega_{\alpha\beta} - \Gamma_{\alpha\beta})\tau_1}, \tag{A10}$$

and the spectrum is given by Eq. (26), namely,

$$F(\omega) = \frac{\pi\omega'}{2\varepsilon_0 V} \sum_{\alpha,\beta} \frac{p_\beta C_{\alpha\beta}}{\Gamma_{\alpha\beta}\Gamma_\alpha^{\text{rad}}} L(\omega' - \omega_{\alpha\beta}, \Gamma_{\alpha\beta}) \big[\Gamma_\alpha^{\text{rad}}\delta(\omega' - \omega) + \Gamma_\alpha^{\text{coll}}L(\omega - \omega_{\alpha\beta}, \Gamma_{\alpha\beta})\big], \tag{A11}$$

where $\Gamma_\alpha^{\text{rad}} = \langle\alpha|K_{\text{rad}}|\alpha\rangle$, $\Gamma_{\alpha\beta}^{\text{coll}} = \langle\alpha|K_{\text{coll}}|\alpha\rangle + \langle\beta|K_{\text{coll}}|\beta\rangle$, and where $L(x,\gamma) = (\gamma/\pi)/(x^2 + \gamma^2)$ denotes the normalized Lorentzian function. Note that $\langle\beta|K_{\text{rad}}|\beta\rangle$ has here been set equal to zero since the lower level is not subject to radiative decay for Lyman lines.

[1] D. Mihalas, *Stellar Atmospheres* (W. H. Freeman, San Francisco, 1978).

[2] V. Bommier, Master equation theory applied to the redistribution of polarized radiation in the weak radiation field limit – V. The two-term atom, Astron. Astrophys. **607**, A50 (2017).

[3] V. Bommier, Master equation theory applied to the redistribution of polarized radiation in the weak radiation field limit – VI. Application to the second solar spectrum of the Na I D1 and D2 lines: Convergence, Astron. Astrophys. **644**, A65 (2020).

[4] R. Casini, M. Landi Degl'Innocenti, R. Manso Sainz, E. Landi Degl'Innocenti, and M. Landolfi, Frequency redistribution function for the polarized two-term atom, Astrophys. J. **791**, 94 (2014).

[5] J. Oxenius, *Kinetic Theory of Particles and Photons—Theoretical Foundations of Non-LTE Plasma Spectroscopy* (Springer-Verlag, Berlin, 1986).

[6] D. G. Hummer, Non-coherent scattering: I. The redistribution functions with Doppler broadening, Mon. Not. R. Astron. Soc. **125**, 21 (1962).

[7] H. A. Scott, Cretin–a radiative transfer capability for laboratory plasmas, J. Quant. Spectrosc. Radiat. Transfer **71**, 689 (2001).

[8] J. L. Kline *et al.*, Progress of indirect drive inertial confinement fusion in the United States, Nucl. Fusion **59**, 112018 (2019).

[9] J.-L. Miquel and E. Prene, LMJ & PETAL status and program overview, Nucl. Fusion **59**, 032005 (2019).

[10] B. A. Remington, R. P. Drake, and D. D. Ryutov, Experimental astrophysics with high power lasers and Z pinches, Rev. Mod. Phys. **78**, 755 (2006).

[11] J. L. Giuliani, G. M. Petrov, J. P. Apruzese, and J. Davis, Non-local radiation transport via coupling constants for the radially inhomogeneous Hg–Ar positive column, Plasma Sources Sci. Technol. **14**, 236 (2005).

[12] J. C. de Aquino Carvalho and T. P. de Silans, Backward fluorescence of optically thick Cs vapor: Experiment and Monte-Carlo simulations, J. Quant. Spectrosc. Radiat. Transfer **260**, 107469 (2021).

[13] N. I. Kosarev, Numerical investigation of the escape factor of lithium and sodium vapour at partial frequency redistribution, J. Phys. B: At., Mol. Opt. Phys. **41**, 225401 (2008).

[14] M. O. Araújo, T. P. de Silans, and R. Kaiser, Lévy flights of photons with infinite mean free path, Phys. Rev. E **103**, L010101 (2021).

[15] A. Omont, E. W. Smith, and J. Cooper, Redistribution of resonance radiation. I. The effect of collisions, Astrophys. J. **175**, 185 (1972).

[16] G. Nienhuis and F. Schuller, Collisional redistribution of fluorescence radiation, Physica B+C **92**, 397 (1977).

[17] D. Voslamber and J.-B. Yelnik, Collisional Redistribution of Weak Resonance Radiation, Phys. Rev. Lett. **41**, 1233 (1978).

[18] K. Burnett, J. Cooper, R. J. Ballagh, and E. W. Smith, Collisional redistribution of radiation. I. The density matrix, Phys. Rev. A **22**, 2005 (1980).

[19] K. Burnett, Collisional redistribution of radiation, Phys. Rep. **118**, 339 (1985).

[20] A. V. Anufrienko, A. L. Godunov, A. V. Demura, Y. K. Zemtsov, V. S. Lisitsa, A. N. Starostin, M. D. Taran, and V. A. Shchipakov, Nonlinear interference effects in Stark broadening of ion lines in a dense plasma, Zh. Eksp. Teor. Fiz. **98**, 1304 (1990) [Sov. Phys. JETP **71**, 728 (1990)].

[21] A. V. Demura, N. Feautrier, I. N. Kosarev, V. S. Lisitsa, and C. Stehlé, Model microfield method for partial redistribution of resonance radiation in dense plasmas, J. Phys. B: At., Mol. Opt. Phys. **31**, 4283 (1998).

[22] C. Mossé, A. Calisti, R. Stamm, B. Talin, R. Lee, and L. Klein, Redistribution of resonance radiation in hot and dense plasmas, Phys. Rev. A **60**, 1005 (1999).

[23] D. Benredjem, C. Mossé, H. Guennou, A. Sureau, A. Demir, B. Talin, and C. Möller, Frequency redistribution in the radiative transfer problem of amplifying media. Application to Ge^{22+} and C^{5+} x-ray lasers, J. Phys. B: At., Mol. Opt. Phys. **33**, 2295 (2000).

[24] A. V. Anufrienko, A. E. Bulyshev, A. L. Godunov, A. V. Demura, Yu. K. Zemtsov, V. S. Lisitsa, and A. N. Starostin, Nonlinear interference effects and ion dynamics in the kinetic theory of Stark broadening of the spectral lines of multicharged ions in a dense plasma, Zh. Eksp. Teor. Fiz. **103**, 417 (1993) [J. Exp. Theor. Phys. **76**, 219 (1993)].

[25] A. E. Bulyshev, A. V. Demura, V. S. Lisitsa, A. N. Starostin, A. E. Suvorov, and I. I. Yakunin, Redistribution function for resonance radiation in a hot dense plasma, Zh. Eksp. Teor. Fiz. **108**, 212 (1995) [J. Exp. Theor. Phys. **81**, 113 (1995)].

[26] A. Loarte *et al.*, Progress in the ITER Physics Basis. Chapter 4: Power and particle control, Nucl. Fusion **47**, S203 (2007).

[27] J. L. Terry, B. Lipschultz, A. Y. Pigarov, S. I. Krasheninnikov, B. LaBombard, D. Lumma, H. Ohkawa, D. Pappas, and M. Umansky, Volume recombination and opacity in Alcator C-Mod divertor plasmas, Phys. Plasmas **5**, 1759 (1998).

[28] M. L. Adams and H. A. Scott, Effect of hydrogen line radiation on the divertor target plate incident heat flux, Contrib. Plasma Phys. **44**, 262 (2004).

[29] V. Kotov, D. Reiter, A. S. Kukushkin, H. D. Pacher, P. Börner, and S. Wiesen, Radiation absorption effects in B2-EIRENE divertor modelling, Contib. Plasma Phys. **46**, 635 (2006).

[30] E. Marenkov, S. Krasheninnikov, and A. Pshenov, Multi-level model of radiation transport in inhomogeneous plasma, Contib. Plasma Phys. **58**, 570 (2018).

[31] A. A. Pshenov, A. S. Kukushkin, E. D. Marenkov, and S. I. Krasheninnikov, On the role of hydrogen radiation absorption in divertor plasma detachment, Nucl. Fusion **59**, 106025 (2019).

[32] J. Rosato, M. Koubiti, Y. Marandet, and R. Stamm, Modeling of photon trapping effects in high-density divertor plasmas, J. Quant. Spectrosc. Radiat. Transfer **247**, 106949 (2020).

[33] J. Rosato, D. Reiter, A. Demura, Y. Marandet, C. Mossé, and R. Stamm, An analytical model for the Ly α redistribution function in conditions of tokamak edge plasmas, J. Phys. B: At., Mol. Opt. Phys. **41**, 165701 (2008).

[34] A. Raji, J. Rosato, Y. Marandet, and R. Stamm, New analysis of Balmer line shapes in magnetic white dwarf atmospheres, Eur. Phys. J. D **75**, 63 (2021).

[35] R. Stamm, B. Talin, E. L. Pollock, and C. A. Iglesias, Ion-dynamic effects on the line shapes of hydrogenic emitters in plasmas, Phys. Rev. A **34**, 4144 (1986).

[36] M. Baranger, Problem of overlapping lines in the theory of pressure broadening, Phys. Rev. **111**, 494 (1958).

[37] M. Baranger, *Atomic and Molecular Processes* (Academic, London, 1962).

[38] H. R. Griem, *Plasma Spectroscopy* (McGraw-Hill, New York, 1964).

[39] A. C. Kolb and H. Griem, Theory of line broadening in multiplet spectra, Phys. Rev. **111**, 514 (1958).

[40] P. W. Milonni and W. A. Smith, Radiation reaction and vacuum fluctuations in spontaneous emission, Phys. Rev. A **11**, 814 (1975).

[41] H. J. Kimble and L. Mandel, Time development of the light intensity in resonance fluorescence, Opt. Commun. **14**, 167 (1975).

[42] H. J. Kimble and L. Mandel, Theory of resonance fluorescence, Phys. Rev. A **13**, 2123 (1976).

[43] P. W. Milonni, *The Quantum Vacuum—An Introduction to Quantum Electrodynamics* (Academic, San Diego, 1994).

[44] L. Allen and J. H. Eberly, *Optical Resonance and Two-Level Atoms* (Wiley Interscience, New York, 1975).

[45] G. S. Agarwal, *Quantum Statistical Theories of Spontaneous Emission and their Relation to Other Approaches* (Springer, Berlin, 1974).

[46] R. Stamm, E. W. Smith, and B. Talin, Study of hydrogen Stark profiles by means of computer simulation, Phys. Rev. A **30**, 2039 (1984).

[47] R. Stamm, Y. Botzanowski, V. P. Kaftandjian, B. Talin, and E. W. Smith, Ion-Dynamics Effect on Hydrogenic Stark Profiles in Hot and Dense Plasmas, Phys. Rev. Lett. **52**, 2217 (1984).

[48] M. A. Gigosos, J. Fraile, and F. Torres, Hydrogen Stark profiles: A simulation-oriented mathematical simplification, Phys. Rev. A **31**, 3509 (1985).

[49] E. Stambulchik, S. Alexiou, H. R. Griem, and P. C. Kepple, Stark broadening of high principal quantum number hydrogen Balmer lines in low-density laboratory plasmas, Phys. Rev. E **75**, 016401 (2007).

[50] S. Alexiou, Overview of plasma line broadening, High Energy Density Phys. **5**, 225 (2009).

[51] J. Rosato, Y. Marandet, H. Capes, S. Ferri, C. Mossé, L. Godbert-Mouret, M. Koubiti, and R. Stamm, Stark broadening of hydrogen lines in low-density magnetized plasmas, Phys. Rev. E **79**, 046408 (2009).

[52] J. Halenka, W. Olchawa, J. Madej, and B. Grabowski, Pressure shift and gravitational redshift of Balmer lines in white dwarfs: Rediscussion, Astrophys. J. **808**, 131 (2015).

[53] T. A. Gomez, T. Nagayama, D. P. Kilcrease, M. H. Montgomery, and D. E. Winget, Effect of higher-order multipole moments on the Stark line shape, Phys. Rev. A **94**, 022501 (2016).

[54] J. Rosato, Y. Marandet, and R. Stamm, Quantifying the statistical noise in computer simulations of Stark broadening, J. Quant. Spectrosc. Radiat. Transfer **249**, 107002 (2020).

[55] H. R. Griem, M. Baranger, A. C. Kolb, and G. Oertel, Stark broadening of neutral helium lines in a plasma, Phys. Rev. **125**, 177 (1962).

[56] R. H. Garstang, Atoms in high magnetic fields, Rep. Prog. Phys. **40**, 105 (1977).

[57] E. Stambulchik, E. Kroupp, Y. Maron, and V. Malka, On the stark effect of the O I 777-nm triplet in plasma and laser fields, Atoms **8**, 84 (2020).